

Thermal rate constant calculation using flux–flux autocorrelation functions: Application to $\text{Cl}+\text{H}_2\rightarrow\text{HCl}+\text{H}$ reaction

Haobin Wang, Ward H. Thompson,^{a)} and William H. Miller

Department of Chemistry, University of California, and Chemical Sciences Division, Lawrence Berkeley National Laboratory, Berkeley, California 94720

(Received 17 June 1997; accepted 1 August 1997)

An efficient method was recently introduced by Thompson and Miller [J. Chem. Phys. **106**, 142 (1997)] for calculating thermal rate constants using the flux–flux autocorrelation function with absorbing boundary conditions. The method uses an iterative method to exploit the low rank feature of the Boltzmannized flux operator and subsequently only propagates the eigenvectors that have significant contributions to the rate constant. In the present article, this method is used to calculate the thermal rate constants of the $\text{Cl}+\text{H}_2\rightarrow\text{HCl}+\text{H}$ reaction in the temperature range of 200–1500 °K. Total angular momentum is treated by employing the body-fixed axis frame, both exactly and also via various approximations. Comparisons with previous exact and approximate theoretical results are made. © 1997 American Institute of Physics. [S0021-9606(97)00742-3]

I. INTRODUCTION

In a recent paper¹ Thompson and Miller described a particularly efficient procedure for calculating thermal rate constants for chemical reactions that is both “direct,” i.e., avoids having to solve the state-to-state quantum reactive scattering problem, yet also “correct,” i.e., without inherent approximation. The method is based on the formally exact expression for the rate constant as the time integral of the flux–flux autocorrelation function^{2,3}

$$k(T) = Q_r(T)^{-1} \int_0^\infty dt C_{ff}(t), \quad (1.1a)$$

where

$$C_{ff}(t) = \text{tr} [e^{-\beta\hat{H}/2} \hat{F} e^{-\beta\hat{H}/2} e^{i\hat{H}t/\hbar} \hat{F} e^{-i\hat{H}t/\hbar}], \quad (1.1b)$$

$\beta = (k_B T)^{-1}$, and $Q_r(T)$ is the reactant partition function per unit volume. (We also note work by Light *et al.*⁴ and by Manthe⁵ that has features in common with this approach.) The efficiency of the approach relies on two essential features: (1) The low rank of the Boltzmannized flux operator

$$\hat{F}(\beta) = e^{-\beta\hat{H}/2} \hat{F} e^{-\beta\hat{H}/2}, \quad (1.2)$$

which facilitates the evaluation of the trace in Eq. (1.1b), and (2) the fact that the correlation function decays rapidly to zero so that quantum time evolution is required only for short time.

More specifically, “low rank” means that $\hat{F}(\beta)$ has only a relatively small number of eigenvalues that are significantly different from zero, and the first step of the procedure (*vide infra*) is a Lanczos iteration calculation to find these nonzero eigenvalues and the corresponding eigenvectors. It is only these eigenvectors which must be time-evolved quantum mechanically, and only for the relatively short time of $\sim \hbar\beta$ (if the dynamics does not involve the formation of a collision complex) (e.g., $\hbar\beta \approx 27$ fs for T

$= 300$ °K). This methodology is complementary to that of Seideman, Manthe, and Miller⁶ for the analogous “direct” and “correct” calculation of the *microcanonical* rate, i.e., the cumulative reaction probability $N(E)$. One can of course obtain $k(T)$ from $N(E)$,

$$k(T) = [2\pi\hbar Q_r(T)]^{-1} \int_{-\infty}^{\infty} dE e^{-E/k_B T} N(E), \quad (1.3)$$

but use of this expression requires one to have $N(E)$ over a significant range of E even if $k(T)$ is desired for only one value of T . The present canonical version of the methodology is thus clearly desirable if one wishes to have $k(T)$ for only one (or a few) values of T .

The purpose of this paper is to apply this flux correlation approach to the reaction $\text{Cl}+\text{H}_2\rightarrow\text{HCl}+\text{H}$, which is of importance in the chemistry of the atmosphere.^{7–9} Because it has been well studied experimentally,⁸ and also recently been the subject of extensive state-to-state reactive scattering calculations by Mielke *et al.*^{9(b)} using a newly developed potential-energy surface,^{9(a)} it also serves as an excellent benchmark system to test this new methodology and demonstrate its efficiency. Unlike the earlier work of Thompson and Miller,¹ here we treat nonzero total angular momentum (i.e., $J > 0$) exactly and are thus able to assess the accuracy of some of the approximate ways of treating $J > 0$.

Section II first summarizes the flux–flux autocorrelation function methodology, and Sec. III gives specifics of the calculations (basis sets, angular momentum coupling, etc.). Section IV discusses the results, the comparisons with experiment and the scattering calculations, and the validity of various angular momentum decoupling approximations for this reaction. Section V concludes with a discussion of the efficiency of the methodology and its promise for further application.

II. SUMMARY OF THEORY

With an absorbing potential $\hat{\epsilon}$ included in the real time propagation, the flux–flux autocorrelation function in Eq. (1.1b) becomes

^{a)}Current address: Department of Chemistry and Biochemistry, University of Colorado, Boulder, CO 80309.

$$C_{ff}(t) = \text{tr} [e^{-\beta \hat{H}/2} \hat{F} e^{-\beta \hat{H}/2} e^{i(\hat{H} + i\hat{\epsilon})t/\hbar} \hat{F} e^{-i(\hat{H} - i\hat{\epsilon})t/\hbar}], \quad (2.1a)$$

where

$$\hat{F} = \frac{i}{\hbar} [\hat{H}, \hat{h}(s)], \quad (2.1b)$$

is the flux operator, with $h(s)$ being the usual step-function

$$h(s) = \begin{cases} 1, & s > 0 \\ 0, & s < 0. \end{cases} \quad (2.1c)$$

In this section the various operators are indicated in the usual abstract notation (e.g., \hat{H}, \hat{F}) and vectors in bracket notation, though in practice they are finite matrices and vectors in the basis described in Sec. III. The evaluation of Eq. (2.1a) is divided into two steps. First, a Hermitian Lanczos procedure is used to determine the (small number of) nonzero eigenvalues and corresponding eigenvectors of the Boltzmannized flux operator $\hat{F}(\beta)$, Eq. (1.2). Starting with a random initial vector $|v_0\rangle$, a Lanczos iteration sequence, including reorthogonalization

$$|v_n\rangle = \hat{F}(\beta)|v_{n-1}\rangle - \sum_{k=0}^{n-1} |v_k\rangle \langle v_k | \hat{F}(\beta) | v_{n-1} \rangle, \quad (2.2)$$

for $n = 1, 2, \dots$, is used to generate an orthonormal basis spanning the Krylov subspace $\{|v_0\rangle, \hat{F}(\beta)|v_0\rangle, \hat{F}(\beta)^2|v_0\rangle, \dots, \hat{F}(\beta)^n|v_0\rangle\}$. [The action of the Boltzmann operator $e^{-\beta \hat{H}/2}$ onto a vector, as required in Eq. (2.2), is carried out via the split operator algorithm.] Diagonalization of the Hermitian matrix

$$F_{k,k'}(\beta) \equiv \langle v_k | \hat{F}(\beta) | v_{k'} \rangle, \quad (2.3)$$

then yields the eigenvectors $\{|u_m\rangle\}$ with the largest (in absolute value) eigenvalues $\{f_m\}$, so that $\hat{F}(\beta)$ can be represented in its eigenstate expansion as follows:

$$\hat{F}(\beta) = \sum_m f_m |u_m\rangle \langle u_m|. \quad (2.4)$$

The number of Lanczos iterations required for the convergence of this procedure is essentially the number of nonzero eigenvalues of $\hat{F}(\beta)$ and thus small. In practice one can reject the initial trial vector and use the first one generated from Eq. (2.2) as the starting vector in Lanczos procedure. This will guarantee the Lanczos sequence generates basis vectors with eigenvalues in descending order (of absolute values). One terminates the Lanczos iteration by some *a priori* criterion

$$|f_n| < \text{tol} \cdot |f_1|, \quad (2.5)$$

where f_1 and f_n are eigenvalues associated with the first and the n th Krylov vector, and tol is a convergence parameter normally chosen between 0.1% and 1%.

With $\hat{F}(\beta)$ given by Eq. (2.4), the trace in Eq. (2.1a) becomes

$$C_{ff}(t) = \sum_m f_m \langle u_m(t) | \hat{F} | u_m(t) \rangle, \quad (2.6a)$$

where $\{|u_m(t)\rangle\}$ are the *time-evolved* eigenvectors of $\hat{F}(\beta)$

$$|u_m(t)\rangle = e^{-i(\hat{H} - i\hat{\epsilon})t/\hbar} |u_m\rangle. \quad (2.6b)$$

This time evolution thus constitutes the second step of the present procedure, and it is accomplished by the usual methods of time-dependent wave packet propagation. We have used the split-operator algorithm, but others are also possible. $C_{ff}(t)$ is thus generated step-by-step in time as the time evolution in Eq. (2.6b) is carried out.

Since we are only interested in the time integral of the flux-flux autocorrelation function, alternate expressions can be obtained by integrating Eq. (2.1a) by parts

$$\begin{aligned} \int_0^t dt' C_{ff}(t') &= \text{tr} [\hat{F}(\beta) e^{i(\hat{H} + i\hat{\epsilon})t'/\hbar} \hat{h} e^{-i(\hat{H} - i\hat{\epsilon})t'/\hbar}] + \frac{2}{\hbar} \\ &\times \int_0^t dt' \text{tr} [\hat{F}(\beta) e^{i(\hat{H} + i\hat{\epsilon})t'/\hbar} \hat{\epsilon}_p e^{-i(\hat{H} - i\hat{\epsilon})t'/\hbar}], \end{aligned} \quad (2.7a)$$

or

$$\begin{aligned} \int_0^t dt' C_{ff}(t') &= \text{tr} [\hat{F}(\beta) e^{i(\hat{H} + i\hat{\epsilon})t'/\hbar} \hat{h} e^{-i(\hat{H} - i\hat{\epsilon})t'/\hbar}] - \frac{2}{\hbar} \\ &\times \int_0^t dt' \text{tr} [\hat{F}(\beta) e^{i(\hat{H} + i\hat{\epsilon})t'/\hbar} \hat{\epsilon}_r e^{-i(\hat{H} - i\hat{\epsilon})t'/\hbar}], \end{aligned} \quad (2.7b)$$

where t is large enough for the integral to converge. Though formally equivalent to Eq. (1.1), the above expressions actually provide a numerical advantage if a discrete variable representation (DVR) basis is used, because both \hat{h} and $\hat{\epsilon}_p$ ($\hat{\epsilon}_r$) are diagonal matrices that can be multiplied at negligible cost compared to the full matrix of \hat{F} . If the absorbing potential were set to zero, then the second term in Eq. (2.7) would be zero and the overall expression would reduce to the flux-position autocorrelation function used previously,^{3,10} in this case, however, t cannot be too large or else flux will reach the edge of the DVR grid and undergo unphysical reflections. The presence of the absorbing potential prevents such reflections, and in this case the first term vanishes in the $t \rightarrow \infty$ limit, i.e., all of the contribution comes from the second term in Eq. (2.7), the flux “picked up” by the absorbing region, similar in the spirit of the flux cross-correlation function used by Germann *et al.* for the O+OH→O₂+H reaction.¹¹ This is numerically more stable in the case of extensive recrossings of the dividing surface, where the first term in Eq. (2.7) becomes highly oscillatory. The disadvantage of this approach is that it usually takes some time for the wave packet to reach the absorbing region and the resulting propagation time to obtain converged results is longer than the original flux-flux autocorrelation function method. For a direct reaction, it is preferable to keep *both* terms in Eq. (2.7); i.e., the result converges for shorter values of t than the second term alone. Figure 1 illustrates the contribution of each term of Eq. (2.7), and their sum, versus time for the

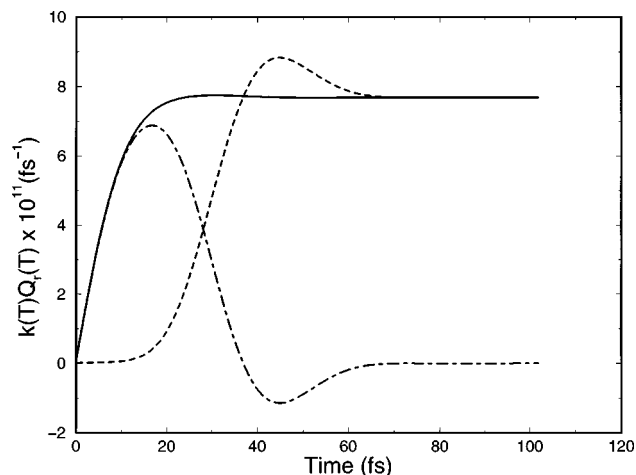


FIG. 1. Contribution of different terms in Eq. (2.7) vs propagation time for the Cl+H₂ reaction at $T=300$ °K and $J=0$. The dot-dashed line is the contribution of the first term in Eq. (2.7) (and goes to zero as $t \rightarrow \infty$), the dashed line is that of the second term (and becomes the correct result as $t \rightarrow \infty$), and the solid line is their sum (which approaches the correct result more rapidly as $t \rightarrow \infty$).

Cl+H₂→HCl+H reaction at $T=300$ °K and $J=0$. One can see that the sum of two terms in Eq. (2.7) converges much more rapidly than the second term alone.

III. DETAILS OF CALCULATION

A. Coordinate system and Hamiltonian

For the Cl+H₂→HCl+H reaction, we have chosen to use the Jacobi coordinates of the Cl+H₂ arrangement since this makes it easier to incorporate the symmetry due to the two identical H atoms. Denoting by r the H–H bond distance, R the distance from Cl to the center-of-mass of H–H, and γ the angle between \mathbf{r} and \mathbf{R} , the total Hamiltonian in the body-fixed frame can be written as¹²

$$\hat{H} = \hat{T}_R + \hat{T}_r + \left(\frac{1}{2\mu R^2} + \frac{1}{2mr^2} \right) \hat{j}^2 + \frac{1}{2\mu R^2} \times (\hat{J}^2 - 2\hat{J}_z^2 + \hat{A} + \hat{B}) + \hat{V}(R, r, \gamma), \quad (3.1a)$$

where

$$\hat{T}_R = -\frac{\hbar^2}{2\mu} \frac{\partial^2}{\partial R^2}, \quad (3.1b)$$

$$\hat{T}_r = -\frac{\hbar^2}{2m} \frac{\partial^2}{\partial r^2}, \quad (3.1c)$$

$$\hat{j}^2 = -\hbar^2 \left(\frac{\partial^2}{\partial \gamma^2} + \cot \gamma \frac{\partial}{\partial \gamma} + \frac{1}{\sin^2 \gamma} \frac{\partial^2}{\partial \psi^2} \right), \quad (3.1d)$$

$$\hat{J}^2 = -\hbar^2 \left[\frac{\partial^2}{\partial \theta^2} + \cot \theta \frac{\partial}{\partial \theta} + \frac{1}{\sin^2 \theta} \times \left(\frac{\partial^2}{\partial \psi^2} + \frac{\partial^2}{\partial \phi^2} - 2 \cos \theta \frac{\partial}{\partial \psi} \frac{\partial}{\partial \phi} \right) \right], \quad (3.1e)$$

$$\hat{J}_z = -i\hbar \frac{\partial}{\partial \psi}, \quad (3.1f)$$

$$\hat{A} = \hbar^2 \left[e^{i\psi} \left(i \cot \theta \frac{\partial}{\partial \psi} - \frac{i}{\sin \theta} \frac{\partial}{\partial \phi} + \frac{\partial}{\partial \theta} \right) \times \left(i \cot \gamma \frac{\partial}{\partial \psi} + \frac{\partial}{\partial \gamma} \right) \right], \quad (3.1g)$$

$$\hat{B} = \hbar^2 \left[e^{-i\psi} \left(i \cot \theta \frac{\partial}{\partial \psi} - \frac{i}{\sin \theta} \frac{\partial}{\partial \phi} - \frac{\partial}{\partial \theta} \right) \times \left(i \cot \gamma \frac{\partial}{\partial \psi} - \frac{\partial}{\partial \gamma} \right) \right]. \quad (3.1h)$$

Here μ is the reduced mass of Cl and H₂, and m that of the two H atoms. (θ, ϕ) are the polar and azimuthal angles which orient \mathbf{R} (which is the body-fixed quantization axis) with respect to a space-fixed axis system, and ψ is the azimuthal angle of \mathbf{r} with respect to \mathbf{R} . \hat{J}^2 is the total angular momentum operator, \hat{J}_z is the projection operator of total angular momentum along the body-fixed axis (\mathbf{R}), and \hat{A} and \hat{B} are Coriolis coupling operators.

The basis for the three Euler angles (ϕ, θ, ψ) is the set of symmetrized Wigner functions

$$\langle \phi \theta \psi | JMK; \sigma \rangle \equiv \frac{1}{\sqrt{2(1 + \delta_{K0})}} [D_{MK}^J(\phi, \theta, \psi) \times (-1)^{J+K+\sigma} D_{M-K}^J(\phi, \theta, \psi)]^*, \quad (3.2)$$

where $\sigma=0$ or 1 is the parity index for the total space inversion and $D_{MK}^J(\phi, \theta, \psi)$ is the usual Wigner function.¹³ J is the total angular momentum quantum number, M the projection of total angular momentum onto the space-fixed axis, and K its projection onto the body-fixed axis (\mathbf{R}). The matrix of \hat{H} with respect to this basis is diagonal in J , M , and σ (and in fact independent of M), but not in K (Ref. 14)

$$\begin{aligned} \langle JMK'; \sigma | \hat{H} | JMK; \sigma \rangle \\ \equiv H_{K',K}^{J,\sigma} = \delta_{K',K} \left\{ \hat{T}_R + \hat{T}_r + \hat{T}_\gamma + \hat{V}(R, r, \gamma) + \frac{\hbar^2}{2\mu R^2} \right. \\ \left. \times [J(J+1) - 2K^2] \right\} \\ - \frac{\hbar}{2\mu R^2} (\delta_{K',K+1} \sqrt{1 + \delta_{K,0}} \Lambda_{JK}^+ \hat{j}_+ \\ + \delta_{K',K-1} \sqrt{1 + \delta_{K,1}} \Lambda_{JK}^- \hat{j}_-), \end{aligned} \quad (3.3a)$$

where

$$\hat{T}_\gamma = \left(\frac{1}{2\mu R^2} + \frac{1}{2mr^2} \right) \hat{j}^2, \quad (3.3b)$$

$$\Lambda_{JK}^\pm = \sqrt{J(J+1) - K(K \pm 1)}. \quad (3.3c)$$

The parity σ determines the range of K and K' , i.e., when $J+\sigma$ is even, $K, K'=0, \dots, J$ and otherwise $K, K'=1, \dots, J$. The operators \hat{j}^2 and \hat{j}_{\pm} are defined by

$$\hat{j}^2 = -\hbar^2 \left(\frac{\partial^2}{\partial \gamma^2} + \cot \gamma \frac{\partial}{\partial \gamma} - \frac{K^2}{\sin^2 \gamma} \right), \quad (3.4a)$$

$$\hat{j}_{\pm} = -\hbar \left(\pm \frac{\partial}{\partial \gamma} - K \cot \gamma \right), \quad (3.4b)$$

and satisfy

$$\hat{j}^2 P_j^K(\cos \gamma) = \hbar^2 j(j+1) P_j^K(\cos \gamma), \quad (3.5a)$$

$$\hat{j}_{\pm} P_j^K(\cos \gamma) = \hbar \Lambda_{jK}^{\pm} P_j^{K \pm 1}(\cos \gamma), \quad (3.5b)$$

where $P_j^K(\cos \gamma)$ is the associated Legendre function. Therefore \hat{j}^2 and \hat{j}_{\pm} are not the usual angular momentum operators; they operate only on the associated Legendre function.

B. Basis set

In the present calculation a discrete variable representation (DVR)^{15–17} has been used for the (r, R, γ) degrees of freedom. Specifically, we have used the sinc-function DVR developed by Colbert and Miller¹⁷ for the r and R coordinates. The grid constant N_B , which determines the number of points per thermal de Broglie wavelength

$$\Delta x = \frac{2\pi}{N_B} \left(\frac{2\mu k_B T}{\hbar^2} \right)^{-1/2}, \quad (3.6)$$

was chosen to be 9–14 for the temperature range 300–1500 °K. At $T=200$ °K, we found that N_B had to be as large as 23 to give converged results.

The natural finite basis representation (FBR) for the angular degree of freedom, seen from Eqs. (3.3) to (3.4), is the set of associated Legendre functions $\{P_j^K(\cos \gamma)\}$, but their dependencies on the quantum number K makes it awkward to construct a DVR for the γ degree of freedom in the conventional way (i.e., discretizing the FBR based on associated Legendre quadrature). We have thus used the K -independent grid,^{18,19} i.e., discretizing the FBR using Gauss–Legendre quadrature for all the K -blocks. One can then apply the resulting transformation matrix (rectangular) to construct the DVR from the FBR.²⁰

We have also used symmetrized associated Legendre functions to account for H_2 exchange symmetry

$$\begin{aligned} P_j^{K,p}(\cos \gamma) &= \frac{1}{\sqrt{2}} \{ P_j^K(\cos \gamma) + (-1)^p P_j^{-K}[\cos(\pi - \gamma)] \} \\ &= \frac{1}{\sqrt{2}} [1 + (-1)^{j+p}] P_j^K(\cos \gamma), \end{aligned} \quad (3.7)$$

where $p=0, 1$. The angular kinetic-energy matrices for N symmetrized DVR points, after the procedure described above, are given by

$$\begin{aligned} j_{i',i}^2(p,K) &= \sum_{j=K}^{2N-1} \frac{[1 + (-1)^{j+p}]^2}{2} \{ \sqrt{w_{i'}} P_j^K(\cos \gamma_{i'}) \\ &\quad \times [\hbar^2 j(j+1)] P_j^K(\cos \gamma_i) \sqrt{w_{ij}} \}, \end{aligned} \quad (3.8a)$$

$$\begin{aligned} j_{i',i}^+(p,K) &= \sum_{j=K+1}^{2N-1} \frac{[1 + (-1)^{j+p}]^2}{2} \\ &\quad \times \{ \sqrt{w_{i'}} P_j^{K+1}(\cos \gamma_{i'}) \\ &\quad \times [\hbar \Lambda_{jK}^+] P_j^K(\cos \gamma_i) \sqrt{w_{ij}} \}, \end{aligned} \quad (3.8b)$$

$$j_{i',i}^-(p,K) = j_{i',i}^+(p,K-1). \quad (3.8c)$$

In our calculation, we found $N=8-10$ to be adequate.

In general, one needs to perform calculations for both even and odd parities, i.e., $p=0$ and 1, and the total rate constant is given by

$$k(T) = Q_r(T)^{-1} \int_0^{\infty} dt [g_0 C_{ff}^0(t) + g_1 C_{ff}^1(t)], \quad (3.9a)$$

where $C_{ff}^p(t)$ is the flux correlation function for parity p , and

$$Q_r(T) = g_0 Q_r^0(T) + g_1 Q_r^1(T), \quad (3.9b)$$

where $Q_r^p(T)$ is the reactant partition function for parity p , g_p being the nuclear spin degeneracy factor for even and odd parities (in the present case 1 and 3 for $p=0$ and 1, respectively). However, the transition state for Cl+H₂ reaction is very tight and has a high barrier for H₂ internal rotation. Therefore the tunneling splittings for H₂ internal rotation at the transition state are small, and one expects the time integral of the flux correlation functions for even and odd parities to be similar. This is indeed what we have found. Similar behavior had also been found for the cumulative reaction probabilities.^{9(b)} This property is used in the actual calculation to reduce the computational cost by half.

Finally, the primitive set of grid points is truncated by discarding grid points for which the potential energy is greater than some cutoff value V_{cut} and those that lie beyond the boundary of the absorbing potential.

C. Approximations for $J>0$

The rate constant calculation described above needs to be carried out for each value of total angular momentum J , yielding $k_J(T)$, and then the total rate constant is given by

$$k(T) = \sum_{J=0} (2J+1) k_J(T), \quad (3.10)$$

where the factor $2J+1$ is from the sum over the space-fixed projection quantum number M . The exact treatment of angular momentum requires including the diagonal and off-diagonal K -states in the calculation, as described in Secs. III A and III B. In practice, however, the contribution dies off rapidly with increasing K , so that only K -states up to $K_{\text{max}}=3$ are necessary to achieve convergence even for large J . The calculation of $k_J(T)$ for each J is therefore about an order of magnitude more expensive than the $J=0$ calculation.

The usual helicity conserving approximation (HCA)²¹ corresponds to neglecting the off diagonal, $K' \neq K$, matrix elements in Eq. (3.3), whereby K becomes a “good quantum number.” For each (J, K) one thus carries out a calculation—which is essentially equivalent in difficulty to the $J=0$ calculation—to obtain $k_{JK}(T)$, and then within this approximation

$$k_J^{\text{HCA}}(T) = \sum_{K=-J}^J k_{JK}(T). \quad (3.11)$$

Again, only K states up to K_{max} are necessary for convergence.

The usual HCA, however, does not work very well for the present Cl+H₂ reaction. In general a better approximation of this type is the one suggested by McCurdy and Miller²² which is based on the instantaneous principal axes of the three-atom system. Specifically, the body-fixed quantization axis is chosen to be the instantaneous axis with the smallest moment of inertia, and the HCA made with this choice. The Hamiltonian for this principal axis helicity conserving approximation (PA/HCA) is

$$\hat{H}^{JK} = \hat{H}_0 + E_{\text{rot}}^{JK}(r, R, \gamma), \quad (3.12a)$$

where \hat{H}_0 is the $J=0$ Hamiltonian

$$\begin{aligned} \hat{H}_0 = & \frac{\hbar^2}{2\mu} \frac{\partial^2}{\partial R^2} - \frac{\hbar^2}{2m} \frac{\partial^2}{\partial r^2} - \hbar^2 \left(\frac{1}{2\mu R^2} + \frac{1}{2mr^2} \right) \\ & \times \left(\frac{\partial^2}{\partial \gamma^2} + \cot \gamma \frac{\partial}{\partial \gamma} \right) + V(r, R, \gamma), \end{aligned} \quad (3.12b)$$

and $E_{\text{rot}}^{JK}(r, R, \gamma)$ is the rotational energy of a symmetric top (determined by geometry r, R, γ)

$$\begin{aligned} E_{\text{rot}}^{JK}(r, R, \gamma) = & 1/2[A(r, R, \gamma) + B(r, R, \gamma)] \\ & \times [J(J+1) - K^2] + C(r, R, \gamma)K^2, \end{aligned} \quad (3.12c)$$

where A, B , and C are given in terms of the principal moments of inertia in the usual way (i.e., $A = \hbar^2/2I_A$, etc.). For the present three-atom system these moments of inertia are

$$\begin{aligned} I_C(r, R, \gamma) = & 1/2(\mu R^2 + mr^2) - 1/2[(\mu R^2) + (mr^2) \\ & + 2\mu R^2 mr^2 \cos 2\gamma]^{1/2}, \end{aligned} \quad (3.13a)$$

$$\begin{aligned} I_B(r, R, \gamma) = & 1/2(\mu R^2 + mr^2) + 1/2[(\mu R^2)^2 + (mr^2)^2 \\ & + 2\mu R^2 mr^2 \cos 2\gamma]^{1/2}, \end{aligned} \quad (3.13b)$$

$$I_A(r, R, \gamma) = I_B + I_C = \mu R^2 + mr^2. \quad (3.13c)$$

$E_{\text{rot}}^{JK}(r, R, \gamma)$ is thus essentially a centrifugal potential that adds to the $J=0$ Hamiltonian, Eq. (3.12b), and in the language of spectroscopy one notes that it includes centrifugal distortion (because the rotation constants vary with internal geometry) but neglects Coriolis coupling. This approximation has also been re-discovered more recently by Bowman²³ (termed by him the “adiabatic rotation approximation”) and used quite successfully for determining energies of bound and metastable states of the HCO system.

The simple J -shifting approximation (JSA)²⁴ results if one takes the three rotation constants in Eq. (3.12c) to be constant, i.e., independent of (r, R, γ) , A^\ddagger , B^\ddagger , and C^\ddagger . These are typically the rotation constants evaluated at some reference geometry (e.g., the transition state). The rotational energy of Eq. (3.12c) then enters the Hamiltonian of Eq. (3.12a) as a constant, so that

$$k_{JK}^{JS}(T) = k_0(T) e^{-E_{\text{rot}}^{JK}/k_B T}, \quad (3.14a)$$

with

$$E_{\text{rot}}^{JK} = 1/2(A^\ddagger + B^\ddagger)[J(J+1) - K^2] + C^\ddagger K^2, \quad (3.14b)$$

where $k_0(T)$ is the $J=0$ rate constant. In this case the sums over J and K can be carried out to give

$$k^{JS}(T) = k_0(T) Q_{\text{rot}}^\ddagger(T) \quad (3.15a)$$

where

$$Q_{\text{rot}}^\ddagger(T) = \sum_{J,K} e^{-E_{\text{rot}}^{JK}/k_B T}. \quad (3.15b)$$

Finally, we note that the transition state for the Cl+H₂ reaction is linear, so that $C^\ddagger = \infty$, requiring that $K=0$.

D. Time propagation

The split operator algorithm has been used for both imaginary (Boltzmann operator) and real time propagation. The details have been given previously¹ and will not be repeated here. We only emphasize that for both $J=0$ and the helicity conserving approximation case, the angular kinetic-energy operator, \hat{T}_γ , is diagonal in the FBR. To form the propagator in the DVR, one only needs to exponentiate \hat{T}_γ in the FBR and then apply the FBR-DVR transformation. When the Coriolis coupling terms are included, the kinetic-energy matrix is block-tridiagonal in the FBR. In principle, to form the propagator using the same strategy, one needs to diagonalize all the (j, K) blocks for $K \leq \min(J, 2N-1)$. As noted, however, the contribution dies off rapidly with increasing K ;²⁰ we found that $K_{\text{max}}=3$ gives results that are accurate to within a few percent error compared with including the full projections, and thus used this value for our thermal rate constant calculation.

E. Dividing surface and absorbing potential

The dividing surface appearing in the \hat{F} and \hat{h} operators is defined by

$$s = r(\text{H}_1 - \text{H}_2) - r(\text{Cl} - \text{H}_2) + 0.77 = 0, \quad (3.16)$$

in atomic units. The absorbing potential is chosen to be a quartic form

$$\epsilon = \lambda \left(\frac{s - s_0}{s_{\text{max}} - s_0} \right)^4, \quad (3.17)$$

where $s_{\text{max}} = \pm 3.5$ bohr and $s_0 = \pm 1.4$ bohr, with “+” denoting the product valley and “−” the reactant valley.

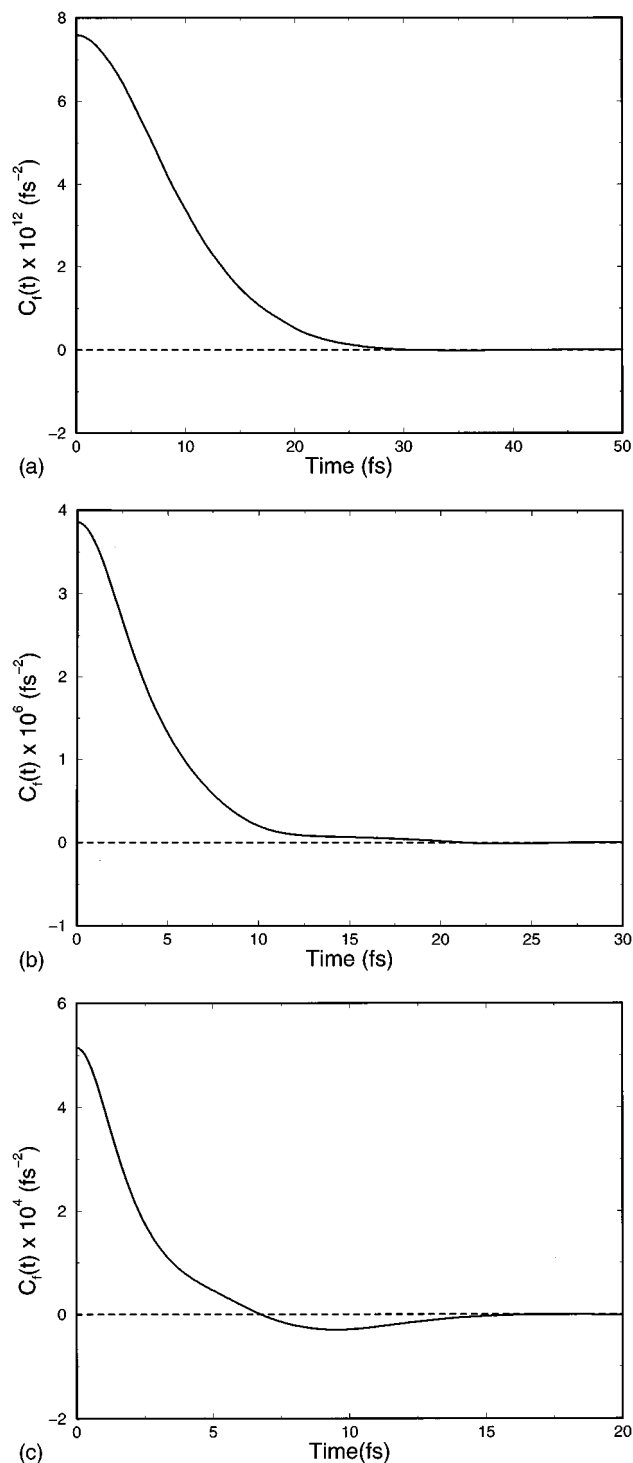


FIG. 2. Flux-flux autocorrelation function for $J=0$ calculation: (a) $T=300$ °K, (b) $T=800$ °K, (c) $T=1500$ °K.

Within a variation of ± 1 bohr, the calculations were insensitive (in terms of both efficiency and accuracy) to the position of dividing surface.

IV. RESULTS

Figure 2 shows the flux-flux autocorrelation function for $J=0$ for several values of temperature T . As expected, for a

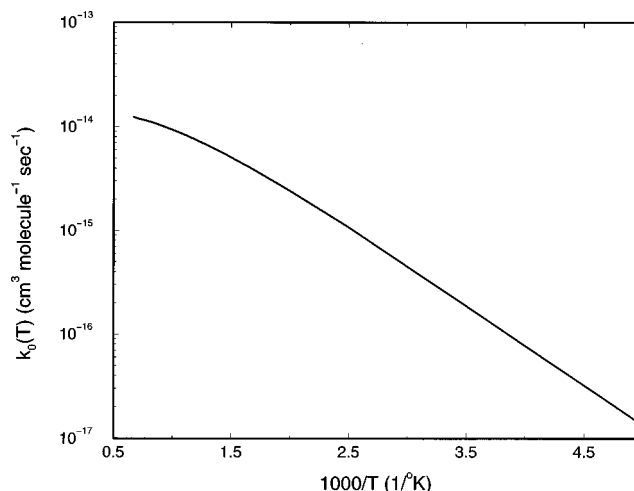


FIG. 3. Arrhenius plot of the thermal rate constants at $J=0$.

direct barrier crossing reaction such as this, $C_f(t)$ falls to zero in a time of order $\hbar\beta$ (≈ 27 fs at 300 °K, ≈ 5 fs at 1500 °K, etc.). This is the type of behavior for which transition state theory is typically an excellent approximation. At the highest temperature in Fig. 2 one does begin to see a small negative lobe in the correlation function, indicative of recrossing flux, i.e., in a classical picture, trajectories that cross the dividing surface more than once and thus cause errors in transition state theory. It is well known²⁵ that these effects in general arise at sufficiently high temperature.

Figure 3 shows the $J=0$ rate constant $k_0(T)$ (i.e., the integral of the correlation functions in Fig. 2) as a function of T . It is very Arrhenius-like, showing some curvature in the high-temperature region, and is in quantitative agreement with the results of Mielke *et al.*^{9(b)} scattering calculations.

Figure 4 shows the J -dependence of $k_J(T)$ for several temperatures; as computed via the exact method described in Sec. III but which is qualitatively the same for the various approximate methods. In the simple J -shifting approximation, Eq. (3.15) show $\ln k_J(T)$ to be a linear function of $J(J+1)$, and Fig. 4 shows that this behavior is a good description of the exact results as soon as J is larger than ~ 3 or 4. This simple dependence on J is extremely useful, of course, for it means that one only needs to carry out calculations, either exactly or approximately, for a few values of J and then interpolate between them in order to evaluate the total rate via Eq. (3.10).

The total rate constants are shown in Fig. 5: The solid line is the result of our full dimensional calculation, i.e., treating $J>0$ exactly as described in Sec. III. Even here, though, we did not carry out the calculations for each value of J , but only at the points shown in Fig. 4 and interpolated to carry out the sum over J . We note that the effective rotation constant obtained from these plots

$$B_{\text{eff}} \equiv -k_B T \frac{d}{d[J(J+1)]} \ln k_J(T), \quad (4.1)$$

increases slightly, from ~ 1.9 to 2.3 cm⁻¹, as T increases from 200 to 1500 °K.

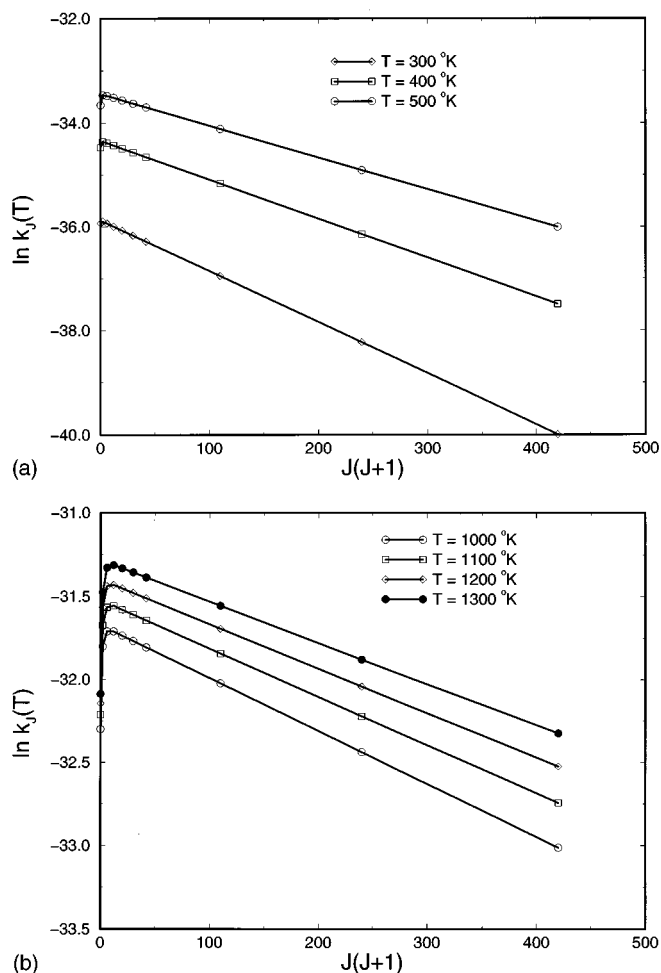


FIG. 4. $\ln k_j(T)$ vs $J(J+1)$ for several temperatures: (a) 300–500 °K, (b) 1000–1300 °K.

The circles in Fig. 5 are the results Mielke *et al.*^{9(b)} obtained via conventional quantum scattering calculations. These authors made explicit calculations for J up to 6 and then extrapolated for higher J using the variational transition state rotation constant $B^\ddagger \approx 2.3 \text{ cm}^{-1}$. One sees that there is excellent agreement between their results and ours, with the slight difference at the lowest temperature being due to their extrapolation of J values.

The dashed line in Fig. 5 shows the results of the simple J -shifting approximation, Eq. (3.15). The agreement with accurate results is excellent at low temperature but progressively degenerates at higher temperature, being a factor of ~ 2.5 too small at 1500 °K. This is primarily due to the fact that this approximation includes only $K=0$, and $K>0$ contributes progressively more as T increases. Nevertheless, for the expense of only the $J=0$ calculation this approximation allows one to obtain an estimate of the complete rate constant and is thus extremely useful (at least for reactions such as this one that are dominated by a single activation barrier).

The triangles in Fig. 5 show the results of the principal axis helicity conserving approximation, Eq. (3.11) with Eqs. (3.12) and (3.13), and they are seen to be in excellent (10% or better over the entire temperature range) agreement with

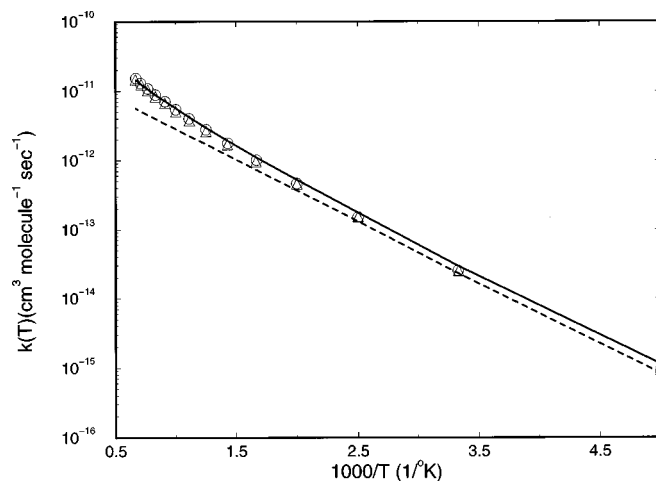


FIG. 5. Arrhenius plot of the thermal rate constants: The solid is the present accurate quantum result, the dashed line is the result of the simple J -shifting approximation, the circles are results from Ref. 9(b), and the triangles are results of the principal axis helicity conserving approximation.

the exact treatment for $J>0$. This is extremely encouraging since the calculation for each J and K is essentially the effort of a $J=0$ calculation. And as noted above, one only needs to carry out calculations for a few values of J and K in order to perform the summation over them to obtain the total rate constant.

Comparison of theoretical results with experiments has been done previously by Mielke *et al.*^{9(b)} Our more accurate quantum calculations does not alter the trend in that comparison, i.e., the theoretical results are larger than the experimental ones at lower temperatures and the agreement gets better at higher temperatures. At this rigorous level of theory, the discrepancies at lower temperatures can only be caused by the inaccuracy of the potential-energy surface, as also pointed out previously.^{9(b)} It would be an interesting future work to apply our method to this reaction using a more accurate potential.

V. CONCLUDING REMARKS

The flux correlation function methodology thus provides an efficient way for calculating rate constants “directly” and “correctly,” as illustrated here for the $\text{Cl} + \text{H}_2 \rightarrow \text{HCl} + \text{H}$ reaction. For simple barrier crossing reactions such as this, the correlation function decays to zero in a very short time. In this case the real time propagation part of the calculation is only slightly more expensive than the evaluation of the Boltzmannized flux operator, which is essentially the calculation performed in a quantum version of transition state theory. (If the reaction dynamics is more complicated, e.g., involving a collision complex,¹¹ then longer time propagation is required. Here, of course, transition state theory is not even approximately correct.)

The calculations presented here are quite efficient and easily implemented. One can utilize the standard methods of time-dependent wave packet propagation for both the imaginary (i.e., Boltzmann operators) and real time propagation. Calculation of the $J=0$ rate constant, $k_0(T)$, requires about

~ 1 – 5 min on an IBM RISC/6000 590 computer. Within the J -shifting approximation—which is of reasonable accuracy except for the highest temperatures—this is essentially all that is needed to obtain the total rate constant $k(T)$. The principal axis helicity conserving approximation—which is quite accurate for all values of T —requires calculations for ~ 8 – 10 values of J and ~ 3 to 4 values of K , each of which is equivalent to a $J=0$ calculation; it is thus ~ 30 times more expensive than the $J=0$ calculation. The fully rigorous treatment of $J>0$ is ~ 100 times the expense of a $J=0$ calculation and is thus still not unduly expensive for the present application. Though the J -shifting approximation only makes sense for the case of a simple barrier crossing reaction—where the reference geometry is that of the transition state—the principal axis helicity conserving approximation should be reasonable much more generally (e.g., even if a collision complex is involved) since the rotation constants vary with geometry (centrifugal distortion).

As with any fully quantum-mechanical calculation, however, the computational expense grows exponentially with the increasing size of the system (i.e., the number of degrees of freedom). One way to escape this dilemma is to exploit the fact that most reactions *effectively* involve only a few degrees of freedom. For the remaining degrees of freedom, reduced-dimensionality approaches can be used to extract a good approximation to the full-dimensional rate constant. There is certainly much to be done to explore such methods. The methodology used in this paper offers a rigorous yet inexpensive treatment of the important degrees of freedom quantum mechanically and should find wide applicability in future work along such directions.

ACKNOWLEDGMENTS

The authors would like to thank Professor Donald Truhlar and Thomas Allison for providing the G3 potential surface for the $\text{Cl} + \text{H}_2$ reaction. They also wish to thank Bill Poirer for many useful discussions. This work was supported by the Director, Office of Energy Research, Office of Basic Energy Sciences, Chemical Sciences Division of the U. S. Department of Energy under Contract No. DE-AC 03-76SF00098, by the Laboratory Directed Research and Development (LDRD) project from National Energy Research Sci-

entific Computing (NERSC) Center, Lawrence Berkeley National Laboratory, and also by National Science Foundation Grant No. CHE 94-22559.

- ¹W. H. Thompson and W. H. Miller, *J. Chem. Phys.* **106**, 142 (1997).
- ²T. Yamamoto, *J. Chem. Phys.* **33**, 281 (1960).
- ³(a) W. H. Miller, *J. Chem. Phys.* **61**, 1823 (1974); (b) W. H. Miller, S. D. Schwartz, and J. W. Tromp, *ibid.* **79**, 4889 (1983).
- ⁴(a) T. J. Park and J. C. Light, *J. Chem. Phys.* **88**, 4897 (1988); (b) D. Brown and J. C. Light, *ibid.* **97**, 5465 (1992).
- ⁵U. Manthe, *J. Chem. Phys.* **102**, 9205 (1995).
- ⁶T. Seideman and W. H. Miller, *J. Chem. Phys.* **96**, 4412 (1992); **97**, 2499 (1992); U. Manthe and W. H. Miller, *ibid.* **99**, 3411 (1993).
- ⁷S. S. Kumaran, K. P. Lim, and J. V. Michael, *J. Chem. Phys.* **101**, 9487 (1994).
- ⁸M. Alagia, N. Balucani, L. Cartechini, P. Casavecchia, E. H. van Kleef, G. G. Volpi, F. J. Aoiz, L. Banares, D. W. Schwenke, T. C. Allison, S. L. Mielke, and D. G. Truhlar, *Science* **273**, 1519 (1996), and references therein.
- ⁹(a) T. C. Allison, G. C. Lynch, D. G. Truhlar, and M. S. Gordon, *J. Phys. Chem.* **100**, 13575 (1996), and references therein; (b) S. L. Mielke, T. C. Allison, D. G. Truhlar, and D. W. Schwenke, *ibid.* **100**, 13588 (1996).
- ¹⁰W. H. Thompson and W. H. Miller, *J. Chem. Phys.* **102**, 7409 (1995).
- ¹¹T. C. Germann and W. H. Miller, *J. Phys. Chem.* (in press).
- ¹²W. H. Miller, *J. Chem. Phys.* **49**, 2373 (1968).
- ¹³M. E. Rose, *Elementary Theory of Angular Momentum* (Wiley, New York, 1967).
- ¹⁴S. E. Choi and J. C. Light, *J. Chem. Phys.* **92**, 2129 (1990). The phase convention we adopt is different from this paper. Therefore as shown in the text, we use the complex conjugate of Wigner function as ‘ket.’
- ¹⁵D. O. Harris, G. G. Engerholm, and W. D. Gwinn, *J. Chem. Phys.* **43**, 1515 (1965).
- ¹⁶(a) J. V. Lill, G. A. Parker, and J. C. Light, *Chem. Phys. Lett.* **89**, 483 (1982); (b) J. C. Light, I. P. Hamilton, and J. V. Lill, *J. Chem. Phys.* **82**, 1400 (1985); (c) J. C. Light, R. M. Whitnell, T. J. Park, and S. E. Choi, NATO ASI Series **277**, 187 (1989).
- ¹⁷D. T. Colbert and W. H. Miller, *J. Chem. Phys.* **96**, 1982 (1992).
- ¹⁸C. Leforestier, *J. Chem. Phys.* **94**, 6388 (1991).
- ¹⁹G. C. Corey and D. Lemoine, *J. Chem. Phys.* **97**, 4115 (1992).
- ²⁰S. M. Auerbach, Ph.D. thesis, Lawrence Berkeley Laboratory, University of California, 1993.
- ²¹R. T. Pack, *J. Chem. Phys.* **60**, 633 (1974).
- ²²C. W. McCurdy and W. H. Miller, *ACS Symp. Ser. No. 56*, edited by P. R. Brooks and E. F. Hayes (American Chemical Society, Washington, D.C., 1977), pp. 239–242.
- ²³(a) J. M. Bowman, *Chem. Phys. Lett.* **217**, 36 (1994); (b) J. Qi and J. M. Bowman, *J. Chem. Phys.* **105**, 9884 (1996).
- ²⁴J. M. Bowman, *J. Phys. Chem.* **95**, 4960 (1991).
- ²⁵(a) P. Pechukas and F. J. McLafferty, *J. Chem. Phys.* **58**, 1622 (1973); (b) S. Chapman, S. M. Hornstein, and W. H. Miller, *J. Am. Chem. Soc.* **97**, 892 (1975).